Effects of ZnO Nanoparticles on Phaseolus vulgaris Germination and Seedling Development Determined by X-ray Spectroscopy

Savassa, Susilaine M.; Duran, Nádia M.; Rodrigues, Eduardo S.; De Almeida, Eduardo; Van Gestel, Cornelis A.M.; Bompadre, Thiago F.V.; De Carvalho, Hudson W.P.

published in
ACS Applied Nano Materials
2018

DOI (link to publisher)
10.1021/acsanm.8b01619

document version
Publisher's PDF, also known as Version of record

ACS APPLIED NANO MATERIALS
Cite This: ACS Appl. Nano Mater. 2018, 1, 6414−6426
Article
www.acsanm.org

Effects of ZnO Nanoparticles on *Phaseolus vulgaris* Germination and Seedling Development Determined by X-ray Spectroscopy

Susilaine M. Savassa,[†] Nádia M. Duran,[†] Eduardo S. Rodrigues,[†] Eduardo de Almeida,[†] Cornelis A. M. van Gestel,[‡] Thiago F. V. Bompadre,[§] and Hudson W. P. de Carvalho*[,†]

[†]Laboratory of Nuclear Instrumentation, Centre for Nuclear Energy in Agriculture, University of São Paulo, Piracicaba, SP 13416000, Brazil

[‡]Department of Ecological Science, Faculty of Science, Vrije Universiteit, De Boelelaan 1085, 1081HV Amsterdam, The Netherlands

[§]Animal Nutrition Laboratory, Centre for Nuclear Energy in Agriculture, University of São Paulo, Piracicaba, SP 13416000, Brazil

Supporting Information

ABSTRACT: There is still little information on the potential use of nanomaterials for seed nutrient enhancement through seed priming. The use of nanoparticles (NPs) in agriculture is promising, but in-depth knowledge on their interaction with plants is required. The aim of this study was to evaluate the effects of different concentrations (1−5000 mg L^{-1}) and sizes (20, 40, and 60 nm) of uncoated ZnO NP compared to ionic $ZnSO_4$ (positive control) on common bean (*Phaseolus vulgaris*) seed germination. The seeds were soaked in ZnO NP aqueous dispersions for 20 min. The ZnO nanoparticles did not affect the germination rate. The 10 mg L^{-1} 40 nm ZnO treatment showed a tendency to increase weight after 5 days (8.26 ± 0.11 g) when compared to the negative control (7.7 ± 0.7 g). However, at 5000 mg L^{-1} 40 nm ZnO NP and $ZnSO_4$ weight was reduced to 7.7 ± 0.8 g and 6.05 ± 0.08 g, respectively. Microprobe X-ray fluorescence showed that most of the Zn absorbed was trapped in the seed coat, while a small fraction entered the cotyledon. X-ray absorption spectroscopy indicated the biotransformation of the ZnO NP. In the hilum and cotyledon, Zn was found associated with organic molecules such as citrate, malate, and histidine-like compounds. Seedling weight reduction depended on the concentration of Zn taken up by the tissue and on the biotransformation of ZnO into organically bound Zn. Considering the properties of the studied NP, in particular the slow Zn release and lower toxicity compared to $ZnSO_4$, the results represent a step forward toward the application of ZnO NP as an agrochemical.

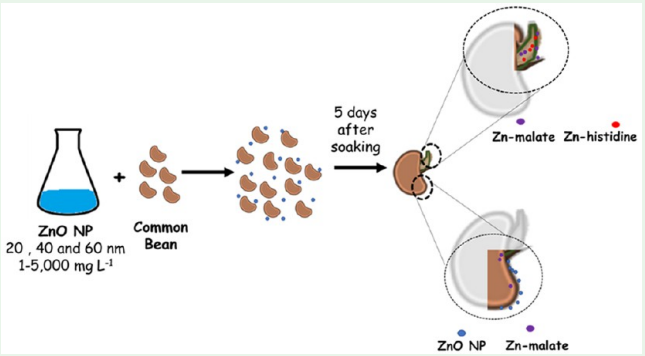

KEYWORDS: *Phaseolus vulgaris, nano ZnO, germination, X-ray absorption spectroscopy, X-ray fluorescence, nanoparticles, seed*

INTRODUCTION

Nearly 49% of worldwide soils are Zn-deficient.[1] This fact reduces agriculture productivity[2,3] afflicting ∼1.1 billion people[4] and makes Zn one of the nutrients with the lowest adequate intake.[5] Seed treatment is a widespread practice that intends to supply micronutrients such as Zn.[6−9] Zinc treatment in cultures of, for instance, rice, wheat, chickpea, maize, and cowpea resulted in grain yield increases varying from ∼6% up to 36% compared to the control plants.[6,10] Specifically for wheat, in calcareous Zn-deficient soils, the grain yield increase promoted by seed priming reached 204%. Several Zn sources can be employed for this purpose, e.g., $ZnSO_4$, Zn-EDTA, and ZnO.[6]

Soluble Zn sources such as sulfates make Zn ions readily available for absorption by plants, while low solubility ZnO can slowly release the nutrient. One has to find a delivering balance responding to the plant demand and avoiding nutrient-induced phytotoxicity. Several studies showed that the solubility of nano-ZnO is affected by particle size.[11−13] Thus, in principle, one could employ ZnO nanoparticles for seed treatment when being able to tune the rate of Zn supply to match with that of plant demand.

Nanomaterials can be absorbed or biotransformed by plants via seeds,[14,15] stomata,[16,17] and roots.[18,13] At first glance, the output of investigations on the effect of nanoparticles (NPs) on plants seems to be contradictory. Positive effects were found for seed germination of *Cicer arietinum* immersed at 2000 mg L^{-1} ZnO NP[19] and on seed germination and seedling vigor of peanut treated with ZnO NP at 1000 mg L^{-1},[20] as well as for tomato treated with carbon nanotubes.[21] Exposure to 6 mg L^{-1} Ag as Ag_2S NP, however, decreased fresh mass of cowpea and wheat, while 0.6 mg L^{-1} Ag as Ag NP reduced their root and shoot growth.[22] Additionally, 125, 250, and 500 mg L^{-1} Ag NP increased water loss in radish, whereas 500 mg

Received: September 14, 2018
Accepted: November 1, 2018
Published: November 1, 2018

DOI: 10.1021/acsanm.8b01619
ACS Appl. Nano Mater. 2018, 1, 6414−6426

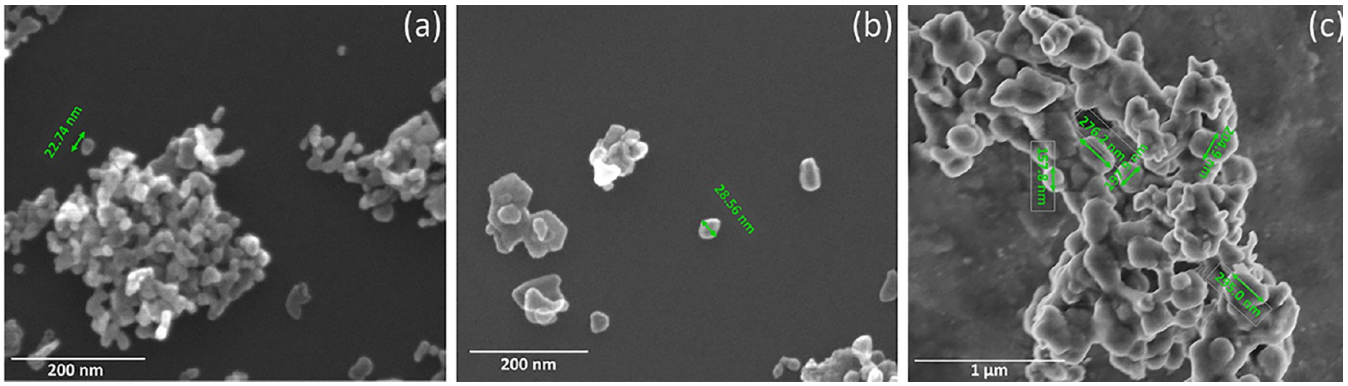

Figure 1. Scanning electron microscopy micrographs of the ZnO NP tested in this study (see Table S1): (a) 20 nm, (b) 40 nm, and (c) 60 nm.

L^{-1} Ag NP decreased root and shoot length.[23] The oxidative stress in rice seedlings depended on CeO_2 NP exposure concentration.[24] In another study, the nutritional value of rice cultivated in soil with 500 mg kg^{-1} CeO_2 NP was modified.[25]

These discrepancies may be caused by the difference in reactivity of the tested nanoparticles, specific properties of each plant species, differences in test media used, the wide range of studied concentrations, and last but not least the lack of a unified protocol for such experiments.

Aside from the environmental concern, nanotechnology might bring benefits for agriculture,[26−28] especially for seed priming. The amount of nutrients available to seeds is a key factor that will influence the germination rate and seedling development.[29,30] To increase their nutrient content and improve germination rate and seedling quality, seeds were soaked for 12 h in 10 mM $ZnSO_4$ and 50 mM KH_2PO_4.[31] However, soaking the seeds in 1000 mM $ZnSO_4$ prevented their germination. The challenge is to supply the right amount of nutrients without losses by leaching and meantime avoid phytotoxicity.

From the physiological perspective, seed germination is a dynamic process of transport, degradation, and syntheses of compounds. First, seed hydration activates the transcription of the DNA region that encodes amylase enzymes. Then, the amylases convert the carbohydrate macromolecules of the seed into maltose. These small sugars act as a source of energy enabling the radicle to emerge and start the germination.[32−34] An important question to be answered is whether and how engineered nanoparticles affect the above-mentioned processes.

X-ray fluorescence (XRF) and absorption (XAS) spectroscopy are powerful tools to evaluate the fate of nanomaterials in biological systems.[35] Zinc presents absorption edge (9659 eV) and emission lines (8640 eV) at energies that make it possible to study this element under air with simple or no sample preparation. XRF yields quantitative information for Zn either by fundamental parameters calculation or calibration curves. XAS is suitable for chemical speciation, which makes it possible to investigate Zn in the local chemical environment. Additionally, the use of microprobe grants analysis with lateral resolution for XRF and XAS.

This study is aimed at investigating whether market available ZnO NPs are toxic or can actually promote the development of plants in their very early stages. A thorough investigation employing X-ray based spectroscopy[35] was performed by examining the effect of ZnO NP on the germination of the common (kidney) bean (*Phaseolus vulgaris*) to uncover the pathways of ZnO NP uptake and biotransformation over a large range of concentrations and particle sizes.

MATERIALS AND METHODS

Nanoparticles and Dispersions Characterization. Three sizes of ZnO NP were used in this study. Powdered NP were purchased from MK Impex Corp. (20 and 40 nm) (Canada) and Nanophase (60 nm) (USA). Bulk ZnO (7 μm) was kindly supplied by Agrichem Company (Brazil). $ZnSO_4{\cdot}7H_2O$ was purchased from MERCK KGaA (Germany) and used as the ionic (Zn^{2+}) treatment.

Energy dispersive X-ray fluorescence spectroscopy (EDXRF) (EDX720, Shimadzu, Japan) was used to determine the chemical composition of the pristine powders. The quantitative method and the chemical composition of the ZnO NP tested and degree of purity of Zn sources are presented in Table S1 in the Supporting Information.

Scanning electron microscopy (SEM; Inspect F50, FEI Company, USA) was employed to image the shape of the nanoparticles (Figure 1). X-ray diffraction (XRD) patterns (Figure S1, Supporting Information) were recorded with a PW 1877 diffractometer (Philips, The Netherlands) using Cu Kα radiation. The crystallite sizes are displayed in Table S2. For these two methods the samples were analyzed in powder form as received from manufacturer.

For germination assays, dissolution tests, hydrodynamic size, ζ potential, conductivity (Supporting Information), and pH measurements the ZnO NPs were dispersed in water. For that, the desired particle mass (1, 10, 100, 1000, or 5000 mg L^{-1}) was stirred in deionized water and sonicated using a probe sonicator (Sonic Dismembrator model 705, Fisher Scientific, USA) for three cycles of 1 min each at 60 W. The solubility of the ZnO NP was evaluated by EDXRF (see the Supporting Information and Figure 2). Hydrodynamic size was determined by dynamic light scattering (DLS), and the ζ potential was estimated using a Zetasizer Nano (Malvern Instruments Ltd., U.K.). The data are presented in Table S3 and Figure S2 of the Supporting Information. The pH and conductivity of NP dispersions and $ZnSO_4$ solutions were measured using the pH/conductivity meter Mettler Toledo SG23, SevenGo Duo model. The ionic strength was estimated using the conductivity values as described in Table S4. In this paper, the concentration of the dispersions, expressed in mg L^{-1}, refers to the mass of ZnO in deionized water. For the $ZnSO_4$ reference compound, the concentration corresponds to the weight of Zn.

Germination Assay. The common bean is an economically important crop and significant source of dietary protein and carbohydrate for many countries. The seeds of *Phaseolus vulgaris* variety BRS Cometa[36] (88% germination rate), obtained from the Brazilian Agricultural Research Corporation (Embrapa), are characterized by a low dormancy level, fast germination, and seedling development. These features make this variety suitable for laboratory experiments.

Deionized water was used as the negative control and aqueous $ZnSO_4$ as the positive control. Seeds were previously weighed and

DOI: 10.1021/acsanm.8b01619
ACS Appl. Nano Mater. 2018, 1, 6414−6426

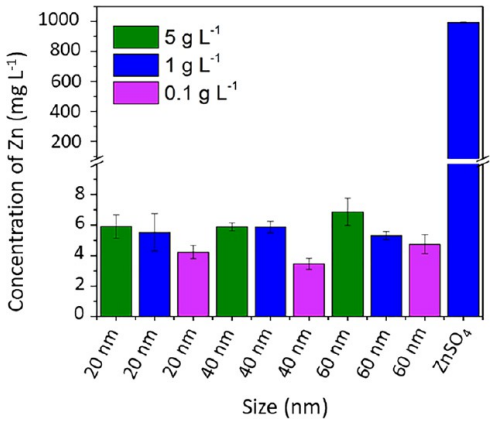

Figure 2. Concentrations of Zn in the supernatant solution of centrifuged dispersions of different ZnO NP and $ZnSO_4$ at different concentrations in deionized water. The measurements were performed in triplicate, and error bars are the standard deviation of the mean.

washed in 10% sodium hypochlorite for 10 s and afterward rinsed in deionized water for another 10 s. Twenty seeds were soaked for 20 min in the dispersions and then transferred to 15 cm Petri dishes covered with filter paper. The paper was moistened with 8 mL of the dispersion. Three replicates were used for each treatment. A plastic film (Parafilm) was used to wrap the dish edges and partially seal the dishes to avoid loss of moisture. The seeds were incubated for 5 days in a dark ventilated germination chamber (TE-4020, Tecnal, Brazil) at 27 °C. Subsequently, the germinated seed (seedling + seed coat) weight gains were determined (difference between the weight before and after 5 days of germination).

Statistical Analysis of Germination and Weight Gain. The germination assays were performed as a completely randomized designed with a factorial arrangement 5 × 5, with five sources of Zn (ZnO 20 nm, ZnO 40 nm, ZnO 60 nm, ZnO 7 μm, and $ZnSO_4$) and five concentrations (1, 10, 100, 1000 and 5000 mg L^{-1}), plus a control group (H_2O). Seventy-eight experimental units were used for the statistical analyses. The model that represents the fixed effects of treatments reads

$$Y_{ijk} = \mu + S_i + C_j + SC_{ij} + e_{ijk}$$

where Y is the dependent variable (weight gain or germination rate), μ is the overall mean, S is the fixed effect of sources of Zn, C is the fixed effect of concentration, SC is the fixed effect of the interaction between source and concentration, and e is the random error assigned for each measurement, assuming that $e = iid \sim N(0,\sigma_e^2)$. Dependent variable measurements were considered as outliers and were deleted from the database once the externally studentized residual was outside the range of −3 to 3.

The residues (observed − predicted) were plotted as a function of the predicted values to check the assumptions of error normality and homoscedasticity. If the assumption of normality failed, the data were mathematically transformed ($\log_{10}(x)$) for the analyses. However, the results presented are based on the original means. The mixed procedure was used and the means were tested by Tukey ($P < 0.05$). The significant variables were also tested for orthogonal contrast of polynomials to determine linear and quadratic effects; if those effects were significant ($P < 0.05$), the model is shown in the results.

Quantification of Zn Uptake and Root SEM Images. The germinated seeds were washed in deionized water to eliminate any externally adsorbed Zn, dried at 60 °C for 48 h, and separated in two fractions: seedling and seed coat. One gram of each fraction was weighed in a previously decontaminated porcelain crucible and placed into a muffle furnace (Fornitec, F-2, Brazil). The temperature was increased at a 100 °C h^{-1} ramp rate up to 500 °C, and the sample was ashed for 12 h. Subsequently, the ashes were dissolved in 5 mL of 1 M HNO_3 and an amount of 950 μL of the digest was transferred into vials to which 50 μL of Ga 1000 mg L^{-1} was added as internal standard. The sample was homogenized on a tube shaker (Marconi MA 162, Brazil). Zn quantification was carried out using external standard calibration.

Afterward, an amount of 15 μL of the sample was pipetted onto a 6.3 window XRF cuvette (no. 3577, Spex Ind. Inc., USA) sealed with 5 μm thick polypropylene film. The sample was dried at 60 °C in a laboratory oven. This procedure was performed twice. The thin-film sample analyses were carried out in triplicate using the same ZnO NP solubility analysis conditions.

Considering the premise that Zn present in the seed coat was adsorbed, we evaluated the affinity of Zn for binding to this tissue using the Freundlich isotherm as explained in ref 37. The amount of adsorbed solute (q_e) was the concentration of Zn determined by XRF, and the equilibrium concentration (C_e) was the content of Zn present in the solution and dispersions.

For SEM, five seedlings treated with 100 and 1000 mg L^{-1} ZnO dispersions were used. The primary root sampled was cross-sectioned below the secondary roots zones. The samples were processed according ref 38. They were fixed using a modified Karnovsky's solution[39] (2.5% glutaraldehyde, 2% paraformaldehyde, 0.05 M cacodylate buffer (pH 7.2), and 0.001 M $CaCl_2$), dehydrated in a graded acetone series (30, 50, 70, 90, and 100%), and critical point drying using CO_2 (Leica CPD300) mounted on aluminum stubs using double-sided carbon tape and gold coated (Bal-tec model SCD 050). Images were captured using a scanning electron microscope (Jeol, JSM IT 300) at 15 kV.

***μ*-XRF and *μ*-XANES.** Microprobe X-ray fluorescence spectroscopy (μ-XRF) (Orbis PC, EDAX, USA) was used to map the 2D spatial distribution of Zn and other elements (Figure S4), the experimental setup is shown in Figure S5. The X-ray was provided with a Rh anode X-ray tube working at 40 kV and 300 μA. A 30 μm X-ray beam for the Mo Kα was produced by a polycapillary optical element. The detection was carried out by a 30 mm^2 silicon drift detector with resolution of 140 eV for Mn Kα. The maps were registered using a matrix of 128 × 100 points. The dwell time was 1 s per pixel, the measurements were performed under vacuum, and the dead time was around 3%. The XRF intensity maps correspond to the net intensity (total Kα peak intensity minus background intensity). The calculation of the concentration of Zn spots in the seed hilum was performed by emission-transmission as explained in the Supporting Information.

Zn K edge microprobe X-ray absorption near edge structure (μ-XANES) was measured at the Brazilian Synchrotron Light Laboratory (LNLS) on the XRF beamline.[40] The beamline was equipped with a bending-magnet, Si (111) double crystal monochromator, KB mirror system resulting in a 20 μm diameter spot size, and silicon drift detector (SDD; KETEK GmbH, Germany). The experimental setup is presented in Figure S6 of the Supporting Information. As the literature shows radiations of 10^7 Gy can damage biological tissues, the seeds were exposed to a dose of maximum ~5 × 10^5 Gy (calculated according to da Cruz et al., 2017).[13] Additionally, we did observe the appearance of new spectral features in subsequently recorded spectra. These two factors suggest no radiation damage, such as induced changes in chemical compounds and cells rupture.[41,42]

Besides the bean seeds, using the microprobe, we measured several Zn reference compounds that were either purchased or prepared in our laboratory according to Sarret et al.[43] Briefly, a 3.15 × 10^{-4} M aqueous solution of $ZnCl_2$ (Exôdo Cientifica, Brazil) and then the ligand in acidic form (histidine (Exôdo Científica, Brazil), malate (Exôdo Científica, Brazil), citrate (J. T. Baker), phosphate (J. T. Baker), phytate (Sigma-Aldrich)) were slowly added in a ratio of 10 mol of ligand/mol of Zn, and finally pH was adjusted to 6 and the mixture was stirred for 2 h. For Zn sulfate (Dinâmica Química Contemporânea LTDA) and acetate (Synth) PA reactants were used as purchased. The solutions were frozen and freeze-dried.

The obtained powders were pelletized in cellulose at 0.2 and 1.0 Zn wt % and were included in the LC analysis as model spectra. To improve the signal-to-noise ratio, three μ-XANES spectra were merged. The energy calibration was done with a reference Zn foil.

DOI: 10.1021/acsanm.8b01619
ACS Appl. Nano Mater. 2018, 1, 6414−6426

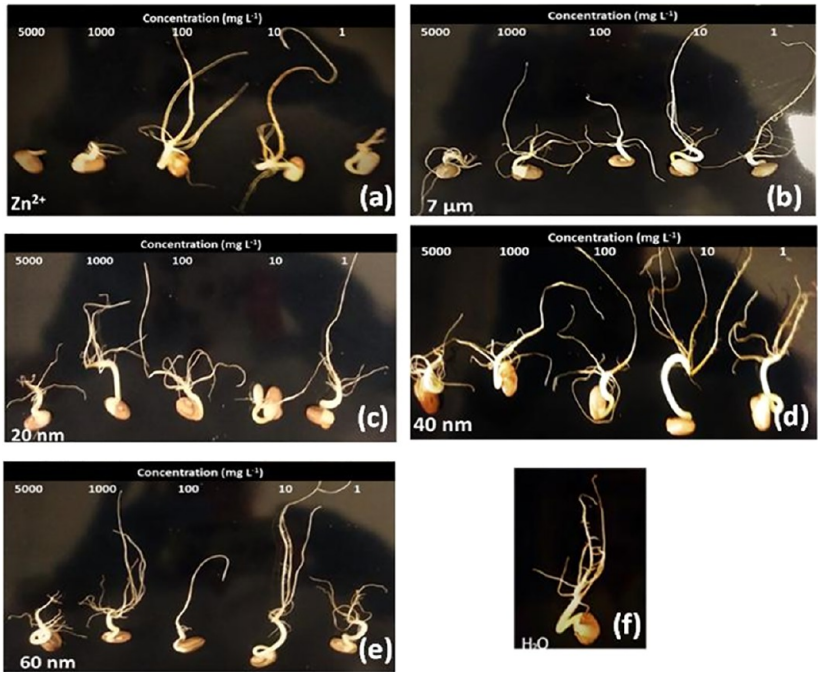

Figure 3. Common bean (*Phaseolus vulgaris*) seedlings after 5 days incubation in a growth chamber: (a) $ZnSO_4$, (b) bulk ZnO, (c) 40 nm ZnO NP, (d) 60 nm ZnO NP, (e) 20 nm ZnO NP, and (f) control (H_2O). Higher concentrations of the treatments prevented proper root development, and lower concentrations such as ZnO 40 nm 10 mg L^{-1} presented one of the biggest root elongation and more lateral roots.

Spectra normalization and linear combination fitting (LCF) analysis were performed through the module Athena in the IFEFFIT package.[44] In the LCF procedure we first choose spectra that presented features similar to those exhibited by the seed samples, and then we evaluated their suitability through a combinatorial fit routine available at the Athena code. The following compounds were tested: Zn-histidine, Zn-malate, Zn-citrate, Zn-acetate, $ZnSO_4$, and ZnO. Finally, aiming at presetting more robust LCF results, we selected the least number of compounds that returned similar *R*-factors. The *R*-factor represents the mismatch between the actual data and the fitted curve, and more details can be found in ref 45.

RESULTS AND DISCUSSION

Nanoparticles and Dispersions Characterization. Nanoparticles were characterized using different techniques. Figure 1 shows micrographs of the 20 nm, 40 nm, and 60 nm ZnO NPs. In the aggregates it is possible to verify different forms in different sizes of nanomaterial. The crystallite size determined by the Scherrer equation using XRD patterns (Figure S1) confirms that 20 nm ZnO NP had a spherical profile (almost same for the all plane sizes). The 40 and 60 nm ZnO NPs showed an elongated form (one plane is different to the others).

It is possible to verify by DLS (Table S3 and Figure S2) that ZnO NP agglomerated in dispersion forming multimodal aggregates. The particle size varied from 124 nm to 5.4 μm. It is important to highlight that the particles were not dispersed by any surfactant. This was done aiming at avoiding the interference of surface agents on the biological results. The ζ-potential measurements showed that regardless of the particle, the surface charge was positive. The low magnitude of the potential, below 30 mV (Table S3), helps to understand the aggregation trend observed by DLS.

The amount of soluble Zn, shown in Figure 2, was determined using EDXRF (method described in the Supporting Information). The ZnO NP dispersions presented similar amounts of soluble Zn regardless of the particle size (4−7 mg Zn L^{-1}). The overlap of the error bars, however, does not allow conclusion that the differences in solubility were a function of particle size. The soluble Zn concentrations were smaller than those reported by Bian et al., who found values from 10 to 57 mg Zn L^{-1} for ZnO particle sizes ranging from 241 nm down to 4 nm.[46] Table S4 presents the pH values of all treatments. For all bulk and nano ZnO suspensions, the pH varied from 6.99 to 7.92 and was not affected by particle concentration. For $ZnSO_4$ treatments, pH decreased from 6.95 to 5.15 as the Zn concentration increased.

Germination Assay. We first determined the effect of ZnO NP size (20 nm, 40 nm, 60 nm, and 7 μm) and concentration (1, 10, 100, 1000, and 5000 mg L^{-1}) on the morphological development of the bean seedlings. Figure 3 shows the root development 5 days after soaking the seeds in the ZnO NP dispersions. For the 40 nm ZnO NP treatment, the most beneficial effect was found at 10 mg L^{-1} which presented one of the biggest elongation rates. All treatments at 5000 mg L^{-1} had deleterious effects on the bean seedlings; the root system was shortened and tangled compared to the negative control and lower concentrations.

Table 1 presents the seed germination rate (%) as a function of treatment. Neither the nanoparticles nor bulk ZnO affected the seed germination rate; i.e., the particle size did not play any role in the effects on germination rate. On the other hand, $ZnSO_4$ at 5000 mg L^{-1} decreased the number of viable seeds. At the germination level, ZnO NP appeared to be less toxic compared to its free ion metal counterpart. This suggests that the deleterious effect is promoted by the excess of zinc ions. The NP released just a small quantity of Zn^{2+} that varied from 3 to 7 mg L^{-1} of Zn.

Table 2 presents the weight gain (g) of seedlings as a function of treatment. The control group (water treatment with weight gain of 7.6 ± 0.4 g) was tested by orthogonal

DOI: 10.1021/acsanm.8b01619
ACS Appl. Nano Mater. 2018, 1, 6414−6426

Table 1. Germination Rate (%) in *Phaseolus vulgaris* Bean Seeds, 5 Days after Treatment with $ZnSO_4$ or Differently Sized ZnO NP and Different Concentrations of Each Source, in the Germination Assay[a]

concn (mg L^{-1})	ZnO 20 nm	ZnO 40 nm	ZnO 60 nm	ZnO 7 μm	$ZnSO_4$	mean[1]
1	78	75	83	88	73^{A}	79
10	68	90	83	78	78^{A}	79
100	78	78	80	81	75^{A}	78
1000	73	85	81	78	71^{A}	78
5000	71^{a}	86^{a}	80^{a}	78^{a}	$48^{A,b}$	73
mean[2]	$74^{A,B}$	83^{A}	81^{A}	81^{A}	69^{B}	

[a]A, B, C: Values followed by different uppercase letters differ in the column (different NP sizes, ZnO bulk and $ZnSO_4$). a,b,c: Values followed by different lowercase letters differ in the row (different concentration, 1−5000 mg L^{-1}). Tukey test (P = 5%). [1]Mean of germination rate values (%) for a defined concentration, i.e., rows. [2]Mean germination rate values (%) given by a defined source of Zn, i.e., columns.

Table 2. Weight Gain of Common Bean Seeds (g) on the Fifth Day of the Germination Assay Following Different Treatments with $ZnSO_4$ or Differently Sized ZnO NP, and Different Concentrations of Each Source[a]

concn (mg L^{-1})	ZnO 20 nm	ZnO 40 nm	ZnO 60 nm	ZnO 7 μm	$ZnSO_4$	mean[1]
1	7.6	7.2^{B}	7.7	8.2^{A}	7.5^{A}	$7.6^{a,b}$
10	7.6	8.3^{A}	7.7	$7.8^{A,B}$	7.8^{A}	7.8^{a}
100	7.6	$7.6^{A,B}$	7.7	$7.5^{A,B}$	7.3^{A}	$7.6^{a,b}$
1000	7.3	$7.7^{A,B}$	7.3	$7.5^{A,B}$	$6.9^{A,B}$	7.3^{b}
5000	$6.9^{a,b}$	$7.0^{A,B,a}$	$7.0^{a,b}$	$7.0^{B,a,b}$	$6.0^{B,b}$	6.9^{b}
mean[2]	$7.39^{A,B}$	7.7^{A}	$7.5^{A,B}$	7.6^{A}	7.1^{B}	

[a]A, B, C: Values followed by different uppercase letters differ in the column (different NP sizes, ZnO bulk and $ZnSO_4$). a, b, c: Values followed by different lowercase letters differ in the row (different concentration, 1−5000 mg L^{-1}). Tukey test (P = 5%). [1]Mean of weight gain values (g) for a defined concentration, i.e., rows. [2]Mean weight gain values (g) given by a defined source of Zn, i.e., columns.

contrast. The results indicated no significant differences among treatments (P = 0.60); therefore the data shown in Table 2 are presented without water treatment. Concerning particle size, the only significant difference was found for 40 nm ZnO and 7 μm ZnO versus $ZnSO_4$. The 40 nm and bulk particles induced the highest weight gain, followed by 60 and 20 nm ZnO. The lowest weight gain was found for $ZnSO_4$. The lower weight gains were associated with the highest concentrations (1000 and 5000 mg L^{-1}). Table S5 shows that for 1 and 10 mg L^{-1} 40 nm ZnO the weight gain could be adjusted by a quadratic function of the treatment concentration.

The seed germination was less sensitive than the seedling weight gain. The concentration of the treatment had more impact on the seedling development than the particle size. Guerinot et al. suggested that under Zn excess some genes, e.g., ZIP1, lose their regulation and affect the metal transporters, leading to toxic effects on the plant.[47] Among the treatments, the highest weight gain was observed for 40 nm ZnO.

Figure 2 shows the lowest solubility (3.5 ± 0.4 mg Zn L^{-1}) for the 40 nm ZnO NP at 100 mg L^{-1} and the highest one (4.8 ± 0.6 mg L^{-1}) for 60 nm ZnO NP at 100 mg L^{-1}. Since $ZnSO_4$ was used as positive control, the observed trend for a beneficial effect of 40 nm ZnO dispersions on seedling development cannot be related to the soluble Zn concentration.

Similar results were presented for *Arabidopsis thaliana*, suggesting that Zn stress can alter the root system architecture.[48] On the other hand, for maize, 10 mg L^{-1} ZnO NP induced the root growth, while 1000 mg L^{-1} ZnO NP was toxic, decreasing germination rate and hindering root development.[49]

Wang et al. reported mass loss of *Arabidopsis* plants treated with 200 mg L^{-1} of ZnO NP.[50] Another study showed that a concentration of 750 mg L^{-1} was highly toxic to rice, reducing germination compared to the control (without ZnO NP). The same happened with the roots that showed size reduction with increasing Zn concentrations.[51] Our results showed that seed priming with ZnO NP up to 100 mg L^{-1} did not harm seedling development. The 40 nm ZnO even presented a trend suggesting a positive effect at 10−100 mg L^{-1}.

Uptake of Zn by Seeds: Quantification and Spatial Distribution. The germinated seeds were washed to remove any excess of Zn from the surface, but since deionized water was used, the procedure did not remove the adsorbed Zn. Then, the germinated seeds were divided into seed coat and seedling (see Figure S7 for details). After dry digestion, they were analyzed by EDXRF. Figure 4a shows the concentration of Zn found in the seed coat and Figure 4b the concentration of Zn in the germinated seed (cotyledon + primary root). The concentration of Zn in both tissues increased as a function of the concentration of the ZnO NP dispersion/solution used for

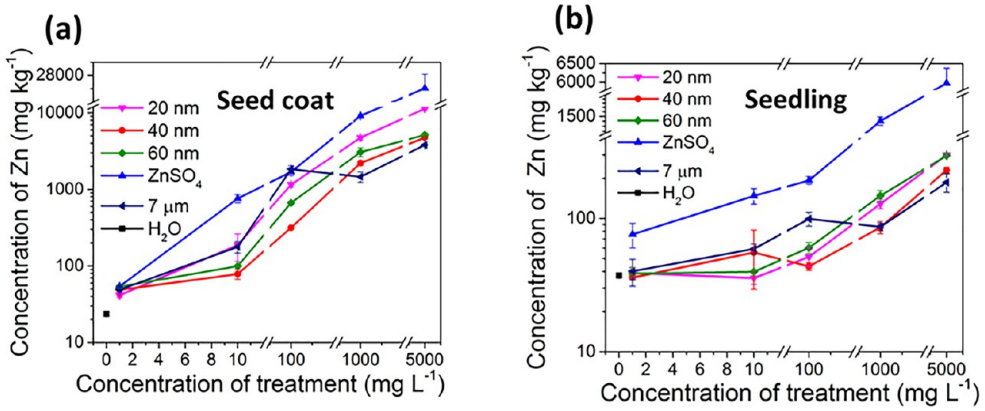

Figure 4. Zinc concentrations, determined using X-ray fluorescence, in the (a) seed coat and (b) seedling of common beans (*Phaseolus vulgaris*) soaked in different concentrations of 20 nm, 40 nm, 60 nm, and 7 μm ZnO NP and $ZnSO_4$.

DOI: 10.1021/acsanm.8b01619
ACS Appl. Nano Mater. 2018, 1, 6414−6426

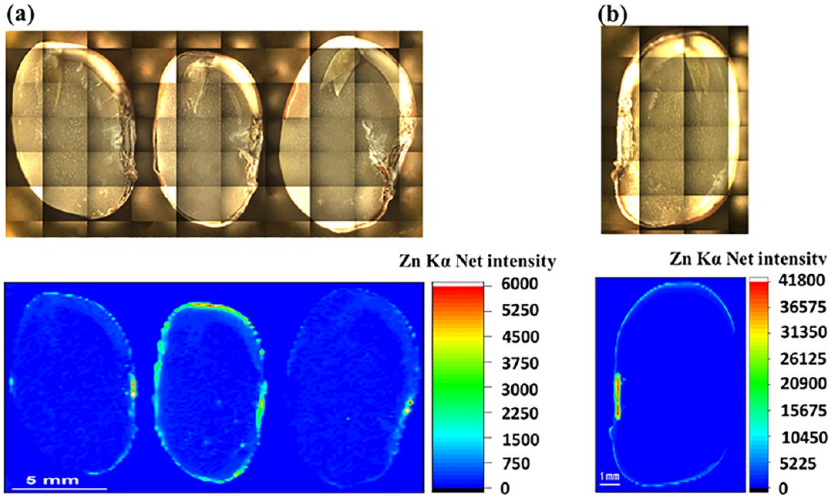

Figure 5. Pictures and zinc mapping of common bean (*Phaseolus vulgaris*) sections exposed to (a) 20, 40, 60 nm ZnO NP and (b) $ZnSO_4$ at 5000 mg L^{-1}. The number of Zn Kα photon counts is directly proportional to the Zn concentration. Zn hotspots were found in the seed coat, especially in the hilum.

priming. The negative control, i.e., the seeds germinated in deionized water, presented Zn concentrations of 24.6 ± 1.2 mg kg^{-1} in the seed coat and 37.4 ± 0.9 mg kg^{-1} in the germinated seedling.

For ZnO NP treated seeds, the seed coat structure retained most of the Zn and had concentrations varying from nearly 50 up to 11 385 mg kg^{-1}. The amplitude of the concentrations presented lower variation in the seedling. In seeds soaked in 1 mg L^{-1} ZnO NP dispersions the Zn did not reach the inner part of the seed.

The data shown in Figure 4a and Figure 4b are also presented without breaks in Figures S8 and S9 of the Supporting Information, respectively. These figures show that the uptake of Zn in the seed coat at different exposure concentrations followed an asymptotic function. A trend of saturation of Zn adsorption sites under high concentrations can be noticed. Figure S10 shows the concentration of Zn in the seedling as a function of the concentration of dissolved Zn. However, it does not show a clear correlation.

One of the simplest mathematical models for adsorption processes revealing constants with physical meaning is the Freundlich isotherm ($x/m = K_f c^{1/n}$), where x is the mass of adsorbate, m is the mass of the substrate, K_f is a measure of the binding strength, and $1/n$ is a measure of the linearity and thus of the concentration dependency of the sorption isotherm.

Due to the restrictions imposed by the experimental conditions of the present work, i.e., the experiments not carried out under isothermal conditions and the equilibrium concentrations not determined, the true Freundlich K and $1/n$ could not be calculated. However, as the log−log plots of the concentration of Zn incorporated in the seed coat versus the concentration of the treatment returned straight lines with correlation coefficients (Pearson's R) higher than 0.95 (see Figure S11), the obtained values were correlated to real Freundlich parameters.

The $1/n$ was similar for ZnO NP and $ZnSO_4$ treatments (Figure S11), but K_f values were between 31.6 and 43.6 $mg^{1-1/n}$ $L^{1/n}$ kg^{-1} for the different ZnO NP and 81.3 $mg^{1-1/n}$ $L^{1/n}$ kg^{-1} for $ZnSO_4$. This indicates that the interaction strength between Zn and the seed coat was higher for $ZnSO_4$ than for the ZnO NP and for the latter not affected by nanoparticle size. This might be related to stronger binding of the ionic Zn compared to the ZnO NP.

Similar data processing and reasoning were followed for the data on Zn found in the germinated seedling. The log−log plots (not presented) showed a constant concentration of Zn in the seedlings for the treatments with ZnO NP between 1 and 100 mg L^{-1}, close to those found in the controls, indicating Zn was mostly trapped in the seed coat. The Zn content in the seedlings increased for ZnO NP treatment levels above 100 mg L^{-1}. In the case of $ZnSO_4$, the uptake of Zn by the inner part of the seed took place through two different regimes.

Figure 5 shows the pictures and the corresponding chemical images of the 2D location of Zn in the beans exposed to 20, 40, 60 nm ZnO NP (Figure 5a) and $ZnSO_4$ (Figure 5b) at 5000 mg L^{-1}. The images corroborate with the data obtained by quantitative EDXRF and show a Zn gradient from the seed coat toward the inner part of the cotyledon. The images also indicate the presence of Zn hotspots in the hilum region. The porous structure of this tissue allows, in addition to other structures, water entrance, radicle hydration, and the beginning of germination.[33] Figure S12 shows the quantitative analysis for a row of 16 points along the hilum region of a seed treated with 5000 mg L^{-1} $ZnSO_4$. The concentration of Zn is not homogeneous, it varied from 184 up to 10902 mg kg^{-1}. The three NP treatments also showed hotspots of Zn accumulation in the hilum region. So together these data show that the hilum structure might be the main entrance of Zn in the seed.

The quantification and chemical images also show that Zn seed priming can transfer the nutrient to the plant through two distinct mechanisms. First, the Zn can be absorbed by cells and might be available for use during germination and the first steps of seedling growth. Second, the Zn stuck to the outer part of the seed coat may be adsorbed by soil colloids and may be available for root absorption later. We did not find any other studies investigating the spatial distribution of Zn in the seed coat after seed priming.

Zinc Speciation. The quantitative assessment of the fraction of Zn species present in the seed is a challenging task. XANES spectra recorded in fluorescence geometry can be distorted by incident beam self-absorption (IBSA) that reduces

DOI: 10.1021/acsanm.8b01619
ACS Appl. Nano Mater. 2018, 1, 6414−6426

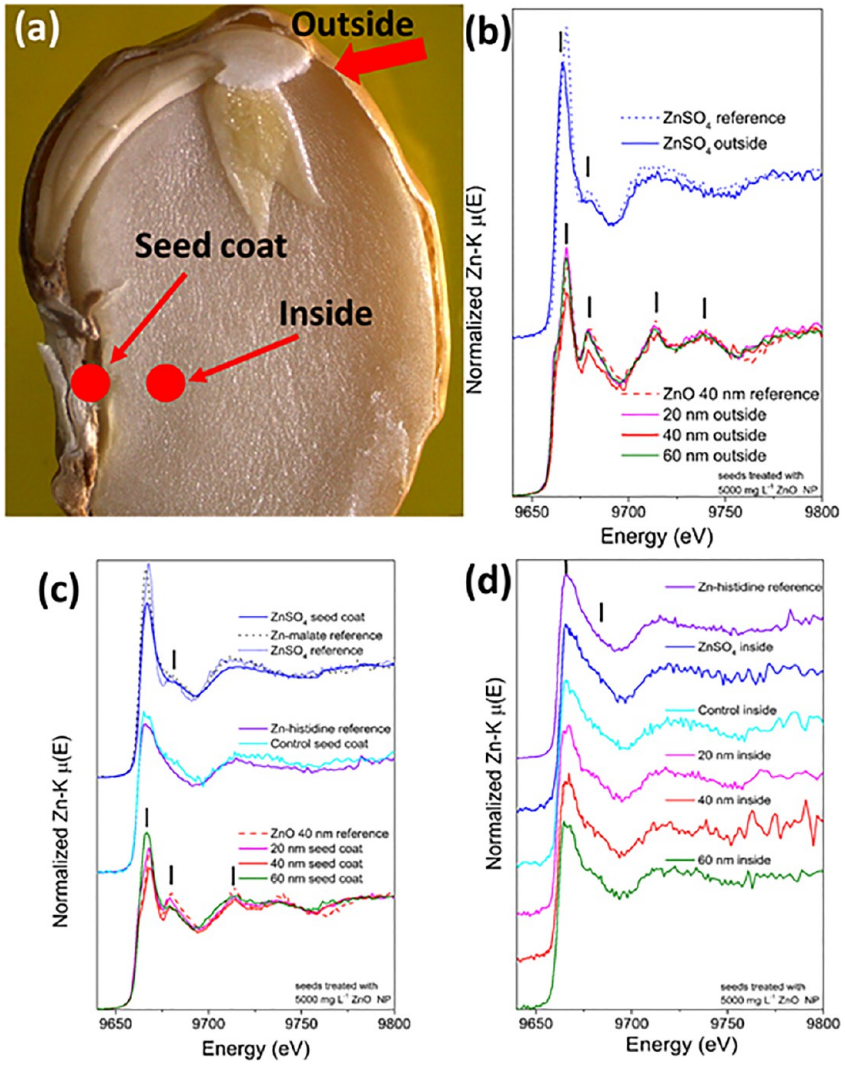

Figure 6. Zn K edge XANES spectra recorded in different regions of common bean (*Phaseolus vulgaris*) seeds treated with 5000 mg L^{-1} dispersions of differently sized ZnO NP and $ZnSO_4$ solution: (a) picture of a bean seed highlighting the regions in which the spectra were recorded; (b) spectra recorded on the outside of the seed; (c) spectra recorded in the seed coat; (d) spectra recorded inside the seed.

the intensity amplitude of the fine structure. As a rule of thumb, it becomes visible when the sample concentration is high enough to record the spectra in transmission geometry (edge jump above ~0.1). Figure S13 illustrates the effect of sample concentration on XANES spectra; it presents the spectra of pelletized Zn organic reference compounds at 0.2 and 1.0 Zn wt %. The energy in which the spectral features arises is the same regardless of the sample concentration; however the intensities of their features, especially the white line (~9668 eV), the shoulder (~9684 eV), and the second absorption crest at ~9617 eV, are reduced in the 1 wt % references. An in-depth discussion of such effect, as well as the strategies to prevent and correct it, is outside the scope of the present study and can be found elsewhere.[52,53] Aiming at avoiding such artifacts, we only performed LCF for the samples whose intensity of the feature at 9617 eV matched those of 0.2 wt % diluted standards. This spectral region was chosen because it is less sensitive to the chemical environment than the absorption edge. For all other samples we qualitatively explored the chemical environment based on the energy of the spectral features.

Another source of error in the LCF is the mismatch between the actual Zn chemical environment of the Zn incorporated by the seeds and that provided by the laboratory synthetized and pelletized reference compounds. Although the linear combination analysis indicated fractions of Zn-malate, it actually means that the Zn embedded in the sample presents a chemical environment similar to that of Zn-malate.

These compromises must be taken into account when investigating such complex biological matrices. In the context of this study, it is more important to unravel whether the incorporated Zn was biotransformed rather than providing the exact weight fractions of its constituents. The speciation was carried out using the seeds soaked in 5000 mg L^{-1} dispersions, which according to Figure 4 yielded Zn concentrations of 0.1–0.3 Zn wt % in the seed coat (except for the $ZnSO_4$ treatment). Additionally, due to the higher Zn concentrations in the sample in the latter treatment, the acquisition time for XANES measurements was shorter so that the sample was exposed to a lower radiation dose.

Figure 6a shows the points where the μ-XANES spectra were recorded for seeds soaked in the 5000 mg L^{-1} ZnO NP and $ZnSO_4$ solutions. The X-ray beam was focused on the

DOI: 10.1021/acsanm.8b01619
ACS Appl. Nano Mater. 2018, 1, 6414–6426

Table 3. Linear Combination Fittings for the XANES Spectra Recorded for Seeds and Seedlings of Common Beans (*Phaseolus vulgaris*) Treated with $ZnSO_4$ and Differently Sized ZnO NP[a]

	percent composition				
analyzed sample region	ZnO	Zn-malate	Zn-histidine	Zn-citrate	*R*-factor ($\times 10^{-3}$)
5000 mg L^{-1} 20 nm seed coat	78 ± 2	22 ± 2			6.9
5000 mg L^{-1} 60 nm seed coat	40 ± 2	60 ± 2			4.8
100 mg L^{-1} 40 nm outside	14 ± 3	86 ± 3			15.0
100 mg L^{-1} 40 nm seed coat, inside	37 ± 2	63 ± 2			8.2
control		34 ± 4	34 ± 5	32 ± 3	9.3
1000 mg L^{-1} 20 nm root		49 ± 4	51 ± 4		12.0
1000 mg L^{-1} 60 nm root		67 ± 3	33 ± 3		8.1

[a] $R\text{-factor} = \frac{\sum(\text{data} - \text{fit})^2}{\sum(\text{data})^2}$. The fitted curves and reference compounds are presented in Figures S13 and S14 in Supporting Information, respectively. Each XANES spectrum was obtained from the merging of three replicate spectra.

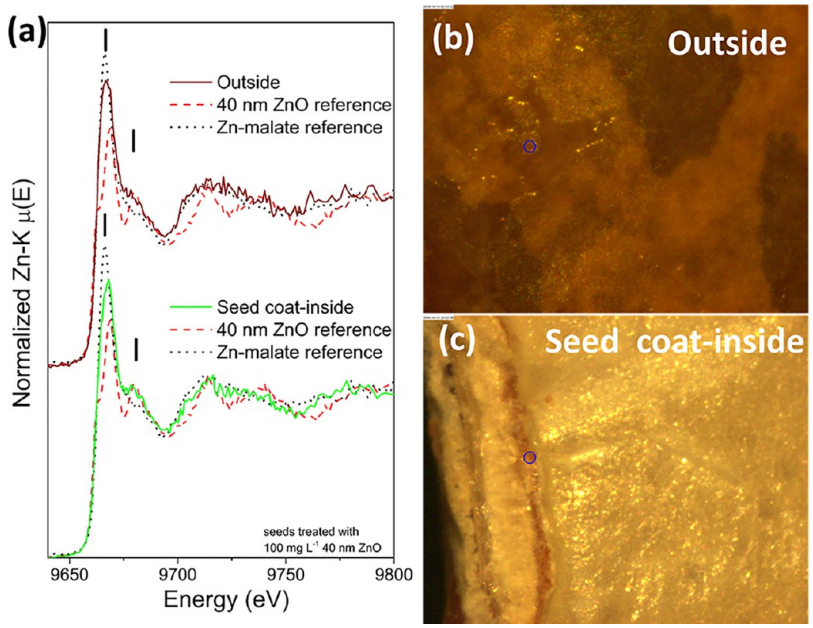

Figure 7. Zn K edge XAS spectra recorded in different regions of common bean (*Phaseolus vulgaris*) seeds treated with a 100 mg L^{-1} 40 nm ZnO NP dispersion: (a) picture of a bean seed highlighting the regions in which the spectra were recorded; (b) spectra recorded on the outside of the bean and in the middle region between the seed coat and the inside.

outside, seed coat (hilum region), and inside the seed, and parts b–d of Figure 6 present the normalized XANES spectra recorded at these regions. The spectral features are a signature of the chemical environment. By overlapping the spectra measured on the sample with those recorded for reference compounds, one can infer the chemical environment of the Zn in the seed.

Figure 6b shows that despite of intensity distortions attributed to ISBA, based on the matching of the energy of spectral features, one can state that the Zn present on the outside did not change compared to the pristine Zn salt and NP. The spectra recorded for $ZnSO_4$ and ZnO NP treated seeds presented similar features as the $ZnSO_4$ and ZnO NP references.

Figure 6c shows the spectra measured on the seed coat. For the sample treated with $ZnSO_4$ the shoulder at 9680 eV is less intense than that of the $ZnSO_4$ reference compound, which suggests a different chemical environment. For the seeds treated with ZnO NP, the features at 9668 and 9679 eV allow detection of the presence of ZnO. The LCF indicated that 20 and 60 nm particles were biotransformed, and the spectra could be fitted as a mixture of ZnO and Zn-malate (Figure S14). The remaining fractions of ZnO were 78 ± 2 and 40 ± 2 for the 20 and 60 nm particles, respectively. The spectrum presented for the control seed presents similar features to that recorded for the Zn-histidine reference compound, which suggests that they have a comparable chemical neighborhood.

Inside the seed (cotyledon) (Figure 6d), regardless of the treatment, the chemical environment of Zn was the same as for the seeds soaked in water, i.e., Zn-histidine-like chemical neighborhood. For the seeds soaked in 5000 mg L^{-1}, the quantitative XRF data showed a concentration of Zn inside the seed ranging from 187 up to 5975 mg kg^{-1}. These values were at least 5-fold higher than those found for the positive control seeds, suggesting biotransformation into Zn-histidine of the Zn incorporated within the seed. This kind of coordination was previously reported for Zn stored in cell vacuoles.[54] Despite the claimed ability of phytic acid to chelate divalent ions,[55] we did not find any evidence of the presence of Zn-\ phytate (spectrum shown in Figure S14a).

Zn-malate reference compound represents a chemical environment in which Zn is surrounded by carboxyl groups,

DOI: 10.1021/acsanm.8b01619
ACS Appl. Nano Mater. 2018, 1, 6414–6426

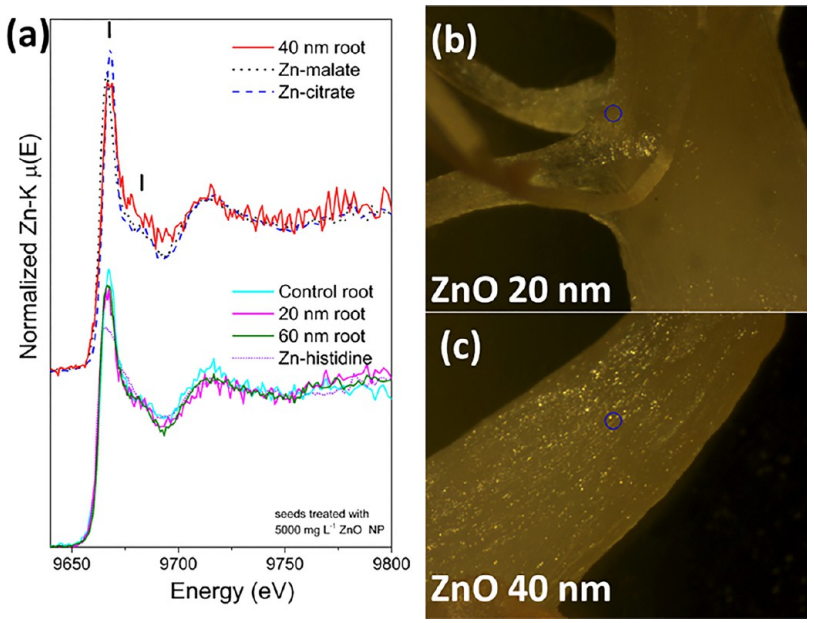

Figure 8. Zn K edge XANES spectra recorded in the root of a common bean (*Phaseolus vulgaris*) seedling on the fifth day of germination following exposure to 1000 mg L^{-1} ZnO NP dispersions. (a) Spectra recorded for a control root, Zn-malate, Zn-citrate and for the seedlings previously treated with 20 nm, 40 nm, and 60 nm ZnO NP. The blue circle in (b) and (c) show the points where the spectra for the 20 nm and 40 nm ZnO were recorded, respectively.

whereas histidine can complex it either via oxygen or nitrogen. Extended X-ray absorption fine structure (EXAFS) analyses showed that Zn-malate is coordinated by four oxygen atoms in the first shell with interatomic distances of 2.01 Å, while the second one is composed by 2 carbon atoms at 2.80 Å.[56] For Zn-histidine, the literature shows four N/O at nearly 2.06 Å and carbon second shell at ~3.00 Å;[57] however it is not clear whether the binding is realized via the carboxyl, amine or imidazole group.

It is important to highlight that other organic acids present in the seed could produce chemical environments similar to those of Zn-malate and Zn-histidine. Although most of the incorporated Zn atoms were binding carboxyl, the presence of ZnO components in the linear combination analysis indicated the possible diffusion of nanoparticles through the spongy hilum tissue.

The seedling weight gain was influenced not only by the Zn concentration of the treatments but also by the size of the particles. Figure S15 presents the seedling weight gain as a function of the Zn concentration in the seed coat (Figure S15a) and in the inner seed part (Figure S15b). Figure S15a shows that the seedling weight gain tended to decrease for Zn concentrations in the seed coat above 1000 mg Zn kg^{-1}. This holds for the $ZnSO_4$ and 20 nm ZnO treatments but not for 40 nm ZnO, even though the seed coat incorporated as much as 4760 ± 140 mg Zn kg^{-1} upon exposure to this nanoparticle size.

The data from Figure S14a combined with the XANES fingerprints suggest that the reduction of weight, i.e., the deleterious effects, did not only depend on the amount of Zn absorbed by the seed. Although it was not possible to quantify the Zn fractions in the 40 nm ZnO treated seed, most of the Zn trapped in the seed coat remained in the ZnO form (Figure 6c), while most of the Zn from $ZnSO_4$ and 20 nm ZnO was biotransformed into an organic Zn form (Figure 6c and Table 3). Therefore, besides being metabolized by seedlings and bound to organic molecules,[58] i.e., malate or histidine, the Zn may also be stored in cell vacuoles and could be used along the plant development.[59]

Figure 7a shows the XANES spectra recorded on the outside of the seed coat and on the interface between seed coat and cotyledon for a seed soaked in the 100 mg L^{-1} 40 nm ZnO NP dispersion. Figure 7b and Figure 7c present pictures indicating the location of the measurements. The spectra uncovered the presence of mixtures of pristine ZnO and Zn-malate (Figure S14a and Figure S14b of the Supporting Information). The relative proportions of the compounds in the mixtures are presented in Table 3.

Different from the seeds soaked in 5000 mg L^{-1} dispersions, the low concentration treatment presented a smaller fraction of ZnO adsorbed on the outside of the seed coat. ZnO was found at the interface of the seed coat cotyledon, which means that nanoparticles could migrate from the dispersion and that part of them were biotransformed. Since ZnO is partially soluble (Figure 2) and some studies even indicate that the solubility increases for nanomaterials, it is still not clear if the biotransformed Zn comes from $Zn_{(aq)}$ that coexisted in dispersion and which was eventually coordinated by the organic compounds.[11] The alternative hypothesis is that ZnO NPs were dissolved inside the hilum and complexed by malate and citrate-like compounds.

The μ-XANES facility was also used to probe the local chemical environment of the Zn in the radicle of seedlings on the fifth day of the germination experiment. Figure 8a presents the spectra recorded for samples treated with 1000 mg L^{-1} ZnO NP dispersions, for a control seedling germinated in water, and for the synthetic Zn-malate, Zn-citrate, and Zn-histidine reference compounds. The linear combination analysis is presented in Table 3, while the fitted spectra are shown in Figure S14 of the Supporting Information.

The non-normalized spectra consistently showed that the amount of Zn was higher in roots of treated seeds compared to

DOI: 10.1021/acsanm.8b01619
ACS Appl. Nano Mater. 2018, 1, 6414−6426

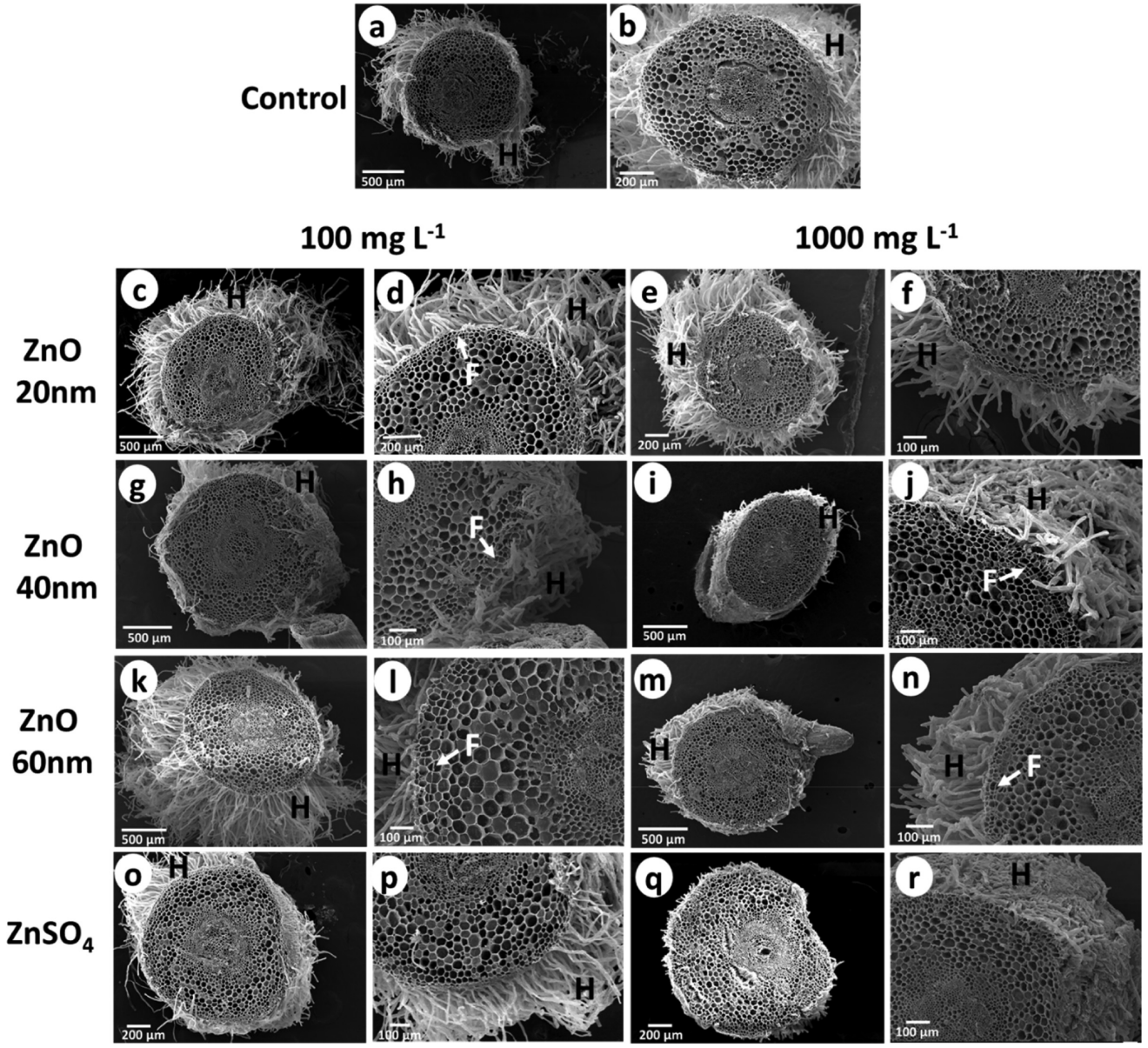

Figure 9. Scanning electron micrographs of transversal section of primary roots of *Phaseolus vulgaris*. The sections were cut 5 days after germination: (a, b) control plants (soaked in water); (c, d) ZnO 20 nm 100 mg L^{-1}; (e, f) ZnO 20 nm 1000 mg L^{-1}; (g, h) ZnO 40 nm 100 mg L^{-1}; (i, j) ZnO 40 nm 1000 mg L^{-1}; (k, l) ZnO 60 nm 100 mg L^{-1}; (m, n) ZnO 60 nm 1000 mg L^{-1}; (o, p) $ZnSO_4$ 100 mg L^{-1}; (q, r) $ZnSO_4$ 1000 mg L^{-1}; H, root hairs; F, felogen.

the control one. The spectra for the control root and that treated with 40 nm ZnO were slightly higher than the line compared to the 20 and 60 nm ZnO treated ones. The spectrum for the control root could only be fitted with the addition of Zn-citrate component. The addition of this third component did not promote a significant decrease of the *R*-factor disagreement parameter.

Even though the seeds were germinated on filter paper moistened with ZnO NP dispersion, the data did not point out the presence of ZnO associated with the root. Such association was shown by Wang et al., who found that ~65% of the Zn present in the roots of *Vigna unguiculata* was in ZnO form when seedling was exposed to a 25 mg L^{-1} ZnO NP dispersion for 4 weeks.[60] In the present study the roots were washed before to the analysis; thus any ZnO adsorbed on the outer part of the root might have been removed.

Figure 9 shows representative SEM images recorded for cross sections of the primary root of *Phaseolus vulgaris* seedling treated with 100 and 1000 mg L^{-1} ZnO dispersions. The treatments did not cause any apparent damage in the cells of cortex and stele regions. On the contrary, the presence of the felogen tissue, i.e., a secondary growth structure, on the treated roots suggests that they developed faster than the control one. The micrographs show changes at the root hairs that are an outgrowth structure from the epidermis cells. The images show that the 100 mg L^{-1} treatments induced the hair growth for ZnO 20 nm (Figure 9c and Figure 9d) and 60 nm (Figure 9h and Figure 9l) compared to the control. Conversely, the 1000 mg L^{-1} treatments decreased the number and length of root hairs, with the exception of ZnO 20 nm (Figure 9h and Figure 9f). The most deleterious treatment was $ZnSO_4$ (Figure 9q

DOI: 10.1021/acsanm.8b01619
ACS Appl. Nano Mater. 2018, 1, 6414−6426

and Figure 9r). It seems that the outer tissues were more affected by the treatments than the inner ones.

Finally, the present study fosters the potential use of NP in plant nutrition. Due to the NP peculiar behavior, it has the potential to act differently from the bulk chemical form, allowing a slower nutrient release compared to salts and faster release compared to the bulk counterpart. It is suitable particularly for micronutrients, in which the amount required is minimum and its toxicity, even at minor levels, is a matter of concern. To the authors' best knowledge, there is no clear sharp reasoning in the literature on the effect of the 20−60 nm nanoparticle size range on seed germination. Since the present work focused on the chemical speciation of Zn present in the seed coat and roots and their effects on total seedling weight gain, additional studies are necessary to uncover the effects of Zn on the development of other seedling parts such as the plumule and embryo axis.

CONCLUSION

The weight gain, after the fifth day of germination, of *Phaseolus vulgaris* bean seeds was unequivocally affected by exposure to 20 nm ZnO NP and $ZnSO_4$ at 5000 mg L^{-1}. None of the other ZnO NP treatments harmed seed germination and seedling development.

At an exposure level of 10 mg L^{-1} of both $ZnSO_4$ and ZnO NP, Zn was transferred to the inner part of the seeds. At 1 mg L^{-1}, the lowest exposure concentration, the Zn provided by the nanoparticles stayed in the seed coat and only in the case of $ZnSO_4$ did the Zn taken up reach the cotyledon.

For all treatments, most of the Zn (51−97%) was trapped in the seed coat. The amount of Zn absorbed by the seed followed an asymptotic function of the concentration, suggesting a saturation of the Zn adsorption sites at high exposure concentrations. The Zn uptake was facilitated for $ZnSO_4$ which is present as Zn^{2+} ions in solution. The μ-XRF showed the presence of Zn hotspots in the hilum region presenting a concentration gradient from the outer to the inner part of the seed.

Zn K edge μ-XANES showed that in the seed coat a fraction of Zn taken up from ZnO NP was present as ZnO, while part was biotransformed to Zn coordinated to organic molecules. The chemical speciation showed that ZnO NP neither entered the cotyledon nor was incorporated into the primary root.

Altogether, at a proper concentration and size, ZnO NP may be a suitable form of Zn to be used for *Phaseolus vulgaris* seed priming. Such ZnO NP form supplied Zn to the bean seeds, and additionally Zn was biotransformed into Zn bound to organic molecules. Compared to $ZnSO_4$ at similar concentrations, the ZnO NP presents the advantage of lower toxicity and provides a slow and controlled Zn delivering. In comparison with the bulk ZnO, the NP has the advantage of a greater active surface, thus minimizing the loss of this finite and limited resource nutrient in crop applications. Additionally, this study only evaluated the ZnO NP effect on the germination stage of the common bean. Further studies monitoring the effects of the treatments on plant development, grain production, Zn content, and speciation in other tissues are currently being carried out by our group and will soon be communicated.

ASSOCIATED CONTENT

Supporting Information

The Supporting Information is available free of charge on the ACS Publications website at DOI: 10.1021/acsanm.8b01619.

Purity analysis of ZnO NP (EDXRF methodology); XRD analysis methodology, X-ray diffraction patterns and crystallite size of the ZnO NP; μ-XRF chemical maps, μ-XRF and μ-XANES experimental setup; TEM images of ZnO NP, ζ potential, hydrodynamic diameter, pH, and conductivity of ZnO NP nanoparticles dispersions; pictures of seedlings; pictures of the two fractions of the germinated seed (seed coat and seedling) analyzed by EDXRF; methodology and quantitative results of the solubility tests carried out with the ZnO NP dispersions and linear combination fittings for Zn K edge XAS spectra (PDF)

AUTHOR INFORMATION

Corresponding Author

*E-mail: hudson@cena.usp.br.

ORCID

Cornelis A. M. van Gestel: 0000-0002-5651-0208

Hudson W. P. de Carvalho: 0000-0003-0875-3261

Notes

The authors declare no competing financial interest.

ACKNOWLEDGMENTS

The authors are grateful for the LNNano (SEM) and LNBio (DLS and ζ potential) facilities. We thank the LNLS for beamtime at XRF beamline (Proposals 20150098, 20160515, and 20160897) and the beamlines scientists Dr. C. A. Perez and Dr. D. Galante for their support at XRF beamline. The authors also thank Dr. J. P. R. Marques for the root SEM images. This study was financed in part by the Coordenação de Aperfeiçoamento de Pessoal de Nivel Superior, Brasil (CAPES), Finance Code 001, Conselho Nacional De Desenvolvimento Científico E Tecnológico, CNPq (Grant 165479/2015-9), FAPESP Young Investigators Award 2015/05942-0, and FAPESP Multiuser Equipment Program 2015/19121-8.

REFERENCES

(1) Sillanpää, M. *Micronutrients and the Nutrient Status of Soils: A Global Study*; Food and Agriculture Organization of the United States, 1982.

(2) Ekiz, H.; Bagci, S. A.; Kiral, A. S.; Eker, S.; Gültekin, I.; Alkan, A.; Cakmak, I. Effects of Zinc Fertilization and Irrigation on Grain Yield and Zinc Concentration of Various Cereals Grown in Zinc-deficient Calcareous Soils. *J. Plant Nutr.* **1998**, *21* (10), 2245−2256.

(3) CAKMAK, I. Tansley Review No. 111. *New Phytol.* **2000**, *146* (2), 185−205.

(4) Kumssa, D. B.; Joy, E. J. M.; Ander, E. L.; Watts, M. J.; Young, S. D.; Walker, S.; Broadley, M. R. Dietary Calcium and Zinc Deficiency Risks Are Decreasing but Remain Prevalent. *Sci. Rep.* **2015**, *5*, 10974.

(5) Beal, T.; Massiot, E.; Arsenault, J. E.; Smith, M. R.; Hijmans, R. J. Global Trends in Dietary Micronutrient Supplies and Estimated Prevalence of Inadequate Intakes. *PLoS One* **2017**, *12* (4), e0175554.

(6) Farooq, M.; Wahid, A.; Siddique, K. H. M. Micronutrient Application through Seed Treatments -a Review. *J. Soil Sci. Plant Nutr.* **2012**, *12* (121), 125−142.

(7) Muhammad, I.; Kolla, M.; Volker, R.; Günter, N. Impact of Nutrient Seed Priming on Germination, Seedling Development,

DOI: 10.1021/acsanm.8b01619
ACS Appl. Nano Mater. 2018, 1, 6414−6426

Nutritional Status and Grain Yield of Maize. *J. Plant Nutr.* **2015**, *38* (12), 1803−1821.
(8) Prom-u-thai, C.; Rerkasem, B.; Yazici, A.; Cakmak, I. Zinc Priming Promotes Seed Germination and Seedling Vigor of Rice. *J. Plant Nutr. Soil Sci.* **2012**, *175* (3), 482−488.
(9) Lavres, J.; Castro Franco, G.; de Sousa Câmara, G. M. Soybean Seed Treatment with Nickel Improves Biological Nitrogen Fixation and Urease Activity. *Front. Environ. Sci.* **2016**, *4*, 37.
(10) Tavares, L. C.; Rufino, C. de A.; Brunes, A. P.; Friedrich, F. F.; Barros, A. C. S. A.; Villela, F. A. Physiological Performance of Wheat Seeds Coated with Micronutrients. *J. Seed Sci.* **2013**, *35*, 28−34.
(11) Mudunkotuwa, I. a; Rupasinghe, T.; Wu, C.-M.; Grassian, V. H. Dissolution of ZnO Nanoparticles at Circumneutral pH: A Study of Size Effects in the Presence and Absence of Citric Acid. *Langmuir* **2012**, *28* (1), 396−403.
(12) Reed, R. B.; Ladner, D. A.; Higgins, C. P.; Westerhoff, P.; Ranville, J. F. Solubility of Nano-Zinc Oxide in Environmentally and Biologically Important Matrices. *Environ. Toxicol. Chem.* **2012**, *31* (1), 93−99.
(13) da Cruz, T. N. M.; Savassa, S. M.; Gomes, M. H. F.; Rodrigues, E. S.; Duran, N. M.; de Almeida, E.; Martinelli, A. P.; de Carvalho, H. W. P. Shedding Light on the Mechanisms of Absorption and Transport of ZnO Nanoparticles by Plants via in Vivo X-ray Spectroscopy. *Environ. Sci.: Nano* **2017**, *4*, 2367.
(14) Ratnikova, T. A.; Podila, R.; Rao, A. M.; Taylor, A. G. Tomato Seed Coat Permeability to Selected Carbon Nanomaterials and Enhancement of Germination and Seedling Growth. *Sci. World J.* **2015**, *2015*, 419215.
(15) Duran, N. M.; Savassa, S. M.; Lima, R. G. de; de Almeida, E.; Linhares, F. S.; van Gestel, C. A. M.; Pereira de Carvalho, H. W. X-ray Spectroscopy Uncovering the Effects of Cu Based Nanoparticle Concentration and Structure on Phaseolus Vulgaris Germination and Seedling Development. *J. Agric. Food Chem.* **2017**, *65*, 7874.
(16) Larue, C.; Castillo-Michel, H.; Sobanska, S.; Trcera, N.; Sorieul, S.; Cécillon, L.; Ouerdane, L.; Legros, S.; Sarret, G. Fate of Pristine TiO2 Nanoparticles and Aged Paint-Containing TiO2 Nanoparticles in Lettuce Crop after Foliar Exposure. *J. Hazard. Mater.* **2014**, *273*, 17−26.
(17) Kim, J.-H.; Oh, Y.; Yoon, H.; Hwang, I.; Chang, Y.-S. Iron Nanoparticle-Induced Activation of Plasma Membrane H+-ATPase Promotes Stomatal Opening in Arabidopsis Thaliana. *Environ. Sci. Technol.* **2015**, *49* (2), 1113−1119.
(18) Hernandez-Viezcas, J. A.; Castillo-Michel, H.; Servin, A. D.; Peralta-Videa, J. R.; Gardea-Torresdey, J. L. Spectroscopic Verification of Zinc Absorption and Distribution in the Desert Plant Prosopis Juliflora-Velutina (Velvet Mesquite) Treated with ZnO Nanoparticles. *Chem. Eng. J.* **2011**, *170* (1−3), 346−352.
(19) Pandey, A. C.; Sanjay, S. S.; Yadav, R. S. Application of ZnO Nanoparticles in Influencing the Growth Rate of Cicer Arietinum. *J. Exp. Nanosci.* **2010**, *5* (6), 488−497.
(20) Prasad, T. N. V. K. V.; Sudhakar, P.; Sreenivasulu, Y.; Latha, P.; Munaswamy, V.; Reddy, K. R.; Sreeprasad, T. S.; Sajanlal, P. R.; Pradeep, T. Effect of Nanoscale Zinc Oxide Particles on the Germination, Growth and Yield of Peanut. *J. Plant Nutr.* **2012**, *35* (6), 905−927.
(21) Khodakovskaya, M. V.; Kim, B. S.; Kim, J. N.; Alimohammadi, M.; Dervishi, E.; Mustafa, T.; Cernigla, C. E. Carbon Nanotubes as Plant Growth Regulators: Effects on Tomato Growth, Reproductive System, and Soil Microbial Community. *Small* **2013**, *9* (1), 115−123.
(22) Wang, P.; Menzies, N. W.; Lombi, E.; Sekine, R.; Blamey, F. P. C.; Hernandez-Soriano, M. C.; Cheng, M.; Kappen, P.; Peijnenburg, W. J. G. M.; Tang, C.; et al. Silver Sulfide Nanoparticles (Ag2S-NPs) Are Taken up by Plants and Are Phytotoxic. *Nanotoxicology* **2015**, *9* (8), 1041−1049.
(23) Zuverza-Mena, N.; Armendariz, R.; Peralta-Videa, J. R.; Gardea-Torresdey, J. L. Effects of Silver Nanoparticles on Radish Sprouts: Root Growth Reduction and Modifications in the Nutritional Value. *Front. Plant Sci.* **2016**, *7*, 90 DOI: 10.3389/fpls.2016.00090.
(24) Rico, C. M.; Hong, J.; Morales, M. I.; Zhao, L.; Barrios, A. C.; Zhang, J.-Y.; Peralta-Videa, J. R.; Gardea-Torresdey, J. L. Effect of Cerium Oxide Nanoparticles on Rice: A Study Involving the Antioxidant Defense System and In Vivo Fluorescence Imaging. *Environ. Sci. Technol.* **2013**, *47* (11), 5635−5642.
(25) Rico, C. M.; Morales, M. I.; Barrios, A. C.; McCreary, R.; Hong, J.; Lee, W.-Y.; Nunez, J.; Peralta-Videa, J. R.; Gardea-Torresdey, J. L. Effect of Cerium Oxide Nanoparticles on the Quality of Rice (Oryza Sativa L.) Grains. *J. Agric. Food Chem.* **2013**, *61* (47), 11278−11285.
(26) Sabir, S.; Arshad, M.; Chaudhari, S. K. Zinc Oxide Nanoparticles for Revolutionizing Agriculture: Synthesis and Applications. *Sci. World J.* **2014**, *2014*, 1.
(27) Peters, R. J. B.; Bouwmeester, H.; Gottardo, S.; Amenta, V.; Arena, M.; Brandhoff, P.; Marvin, H. J. P.; Mech, A.; Moniz, F. B.; Pesudo, L. Q.; et al. Nanomaterials for Products and Application in Agriculture, Feed and Food. *Trends Food Sci. Technol.* **2016**, *54*, 155−164.
(28) Hong, J.; Peralta-Videa, J. R.; Gardea-Torresdey, J. L. Nanomaterials in Agricultural Production: Benefits and Possible Threats? In *Sustainable Nanotechnology and the Environment: Advances and Achievements*; ACS Symposium Series 1124; American Chemical Society, 2013; pp 5−73.
(29) Wang, M.; Tang, X.; Zhang, H.; Zhou, B. Nutrient Enrichment Outweighs Effects of Light Quality in Zostera Marina (Eelgrass) Seed Germination. *J. Exp. Mar. Biol. Ecol.* **2017**, *490* (Suppl. C), 23−28.
(30) Liu, K.; Niu, Y.; Konishi, M.; Wu, Y.; Du, H.; Sun Chung, H.; Li, L.; Boudsocq, M.; McCormack, M.; Maekawa, S.; et al. Discovery of nitrate−CPK−NLP Signalling in Central Nutrient−growth Networks. *Nature* **2017**, *545*, 311.
(31) Ajouri, A.; Asgedom, H.; Becker, M. Seed Priming Enhances Germination and Seedling Growth of Barley under Conditions of P and Zn Deficiency. *J. Plant Nutr. Soil Sci.* **2004**, *167* (5), 630−636.
(32) Ozturk, L.; Yazici, M. A.; Yucel, C.; Torun, A.; Cekic, C.; Bagci, A.; Ozkan, H.; Braun, H. J.; Sayers, Z.; Cakmak, I. Concentration and Localization of Zinc during Seed Development and Germination in Wheat. *Physiol. Plant.* **2006**, *128* (1), 144−152.
(33) Miano, A. C.; Pereira, J. da C.; Castanha, N.; Júnior, M. D. da M.; Augusto, P. E. D. Enhancing Mung Bean Hydration Using the Ultrasound Technology: Description of Mechanisms and Impact on Its Germination and Main Components. *Sci. Rep.* **2016**, *6* (1), 38996.
(34) Iwai, T.; Takahashi, M.; Oda, K.; Terada, Y.; Yoshida, K. T. Dynamic Changes in the Distribution of Minerals in Relation to Phytic Acid Accumulation during Rice Seed Development. *Plant Physiol.* **2012**, *160*, 2007−2014.
(35) Castillo-Michel, H. A.; Larue, C.; Pradas del Real, A. E.; Cotte, M.; Sarret, G. Practical Review on the Use of Synchrotron Based Micro- and Nano- X-Ray Fluorescence Mapping and X-Ray Absorption Spectroscopy to Investigate the Interactions between Plants and Engineered Nanomaterials. *Plant Physiol. Biochem.* **2017**, *110*, 13−32.
(36) de Faria, L. C.; Del Peloso, M. J.; Melo, L. C.; da Costa, J. G. C.; Rava, C. A.; Díaz, J. L. C.; de Faria, J. C.; da Silva, H. T.; Sartorato, A.; Bassinello, P. Z.; et al. CULTIVAR RELEASE-BRS Cometa: A Carioca Common Bean Cultivar with Erect Growth Habit. *Crop Breeding and Applied Biotechnology*; Brazilian Society of Plant Breeding, 2008.
(37) Hamdaoui, O.; Naffrechoux, E. Modeling of Adsorption Isotherms of Phenol and Chlorophenols onto Granular Activated Carbon: Part I. Two-Parameter Models and Equations Allowing Determination of Thermodynamic Parameters. *J. Hazard. Mater.* **2007**, *147* (1), 381−394.
(38) Marques, J. P. R.; Appezzato-da-Glória, B.; Piepenbring, M.; Massola, N. S., Jr; Monteiro-Vitorello, C. B.; Vieira, M. L. C. Sugarcane Smut: Shedding Light on the Development of the Whip-Shaped Sorus. *Ann. Bot.* **2017**, *119* (5), 815−827.
(39) Karnovsky, M. J. A Formaldehyde-Glutaraldehyde Fixative of High Osmolality for Use in Electron Microscopy. *J. Cell Biol.* **1965**, *27*, 137−138.

DOI: 10.1021/acsanm.8b01619
ACS Appl. Nano Mater. 2018, 1, 6414−6426

(40) Pérez, C. A.; Radtke, M.; Sánchez, H. J.; Tolentino, H.; Neuenshwander, R. T.; Barg, W.; Rubio, M.; Bueno, M. I. S.; Raimundo, I. M.; Rohwedder, J. J. R. Synchrotron Radiation X-Ray Fluorescence at the LNLS: Beamline Instrumentation and Experiments. *X-Ray Spectrom.* **1999**, *28* (5), 320−326.
(41) Yano, J.; Kern, J.; Irrgang, K.-D.; Latimer, M. J.; Bergmann, U.; Glatzel, P.; Pushkar, Y.; Biesiadka, J.; Loll, B.; Sauer, K.; Messinger, J.; Zouni, A.; Yachandra, V. K. X-ray Damage to the Mn_4Ca Complex in Single Crystals of Photosystem II: A Case Study for Metalloprotein Crystallography. *Proc. Natl. Acad. Sci. U. S. A.* **2005**, *102* (34), 12047−12052.
(42) James, S. A.; Hare, D. J.; Jenkins, N. L.; de Jonge, M. D.; Bush, A. I.; McColl, G. φXANES: In Vivo Imaging of Metal-Protein Coordination Environments. *Sci. Rep.* **2016**, *6*, 20350.
(43) Sarret, G.; Willems, G.; Isaure, M. P.; Marcus, M. A.; Fakra, S. C.; Frerot, H.; Pairis, S.; Geoffroy, N.; Manceau, A.; Saumitou-Laprade, P. Zinc Distribution and Speciation in Arabidopsis halleri × Arabidopsis lyrata Progenies Presenting Various Zinc Accumulation Capacities. *New Phytol.* **2009**, *184* (3), 581−595.
(44) Ravel, B.; Newville, M. ATHENA, ARTEMIS, HEPHAESTUS: Data Analysis for X-Ray Absorption Spectroscopy Using IFEFFIT. *J. Synchrotron Radiat.* **2005**, *12*, 537−541.
(45) Calvin, S. *XAFS for Everyone*; Taylor & Francis, 2013.
(46) Bian, S.-W.; Mudunkotuwa, I. A.; Rupasinghe, T.; Grassian, V. H. Aggregation and Dissolution of 4 Nm ZnO Nanoparticles in Aqueous Environments: Influence of pH, Ionic Strength, Size, and Adsorption of Humic Acid. *Langmuir* **2011**, *27* (10), 6059−6068.
(47) Guerinot, M. L. The ZIP Family of Metal Transporters. *Biochim. Biophys. Acta, Biomembr.* **2000**, *1465* (1−2), 190−198.
(48) Nair, P. M. G.; Chung, I. M. Regulation of Morphological, Molecular and Nutrient Status in Arabidopsis Thaliana Seedlings in Response to ZnO Nanoparticles and Zn Ion Exposure. *Sci. Total Environ.* **2017**, *575*, 187−198.
(49) Zhang, R.; Zhang, H.; Tu, C.; Hu, X.; Li, L.; Luo, Y.; Christie, P. Phytotoxicity of ZnO Nanoparticles and the Released Zn(II) Ion to Corn (Zea Mays L.) and Cucumber (Cucumis Sativus L.) during Germination. *Environ. Sci. Pollut. Res.* **2015**, *22* (14), 11109−11117.
(50) Wang, X.; Yang, X.; Chen, S.; Li, Q.; Wang, W.; Hou, C.; Gao, X.; Wang, L.; Wang, S. Zinc Oxide Nanoparticles Affect Biomass Accumulation and Photosynthesis in Arabidopsis. *Front. Plant Sci.* **2016**, *6*. DOI: 10.3389/fpls.2015.01243
(51) Salah, S. M.; Yajing, G.; Dongdong, C.; Jie, L.; Aamir, N.; Qijuan, H.; Weimin, H.; Mingyu, N.; Jin, H. Seed Priming with Polyethylene Glycol Regulating the Physiological and Molecular Mechanism in Rice (Oryza sativa L.) under Nano-ZnO Stress. *Sci. Rep.* **2015**, *5* (1), 14278.
(52) Carboni, R.; Giovannini, S.; Antonioli, G.; Boscherini, F. Self-Absorption Correction Strategy for Fluorescence-Yield Soft X-Ray near Edge Spectra. *Phys. Scr.* **2005**, *2005* (T115), 986.
(53) Iida, A.; Noma, T. Correction of the Self-Absorption Effect in Fluorescence X-Ray Absorption Fine Structure. *Jpn. J. Appl. Phys.* **1993**, *32* (6A), 2899.
(54) Küpper, H.; Zhao, F. J.; McGrath, S. P. Cellular Compartimentation of Zinc in the Leaves of the Hyperaccumulator Thlaspi caerulescens. *Plant Physiol.* **1999**, *212*, 75−84.
(55) Lee, C. K.; Karunanithy, R. Effects of Germination on the Chemical Composition of Glycine and Phaseolus Beans. *J. Sci. Food Agric.* **1990**, *51* (4), 437−445.
(56) Sarret, G.; Saumitou-Laprade, P.; Bert, V.; Proux, O.; Hazemann, J.-L.; Traverse, A.; Marcus, M. A; Manceau, A. Forms of Zinc Accumulated in the Hyperaccumulator Arabidopsis halleri. *Plant Physiol.* **2002**, *130* (4), 1815−1826.
(57) Sarret, G.; Manceau, A.; Spadini, L.; Roux, J.-C.; Hazemann, J.-L.; Soldo, Y.; Eybert-BÉrard, L.; Menthonnex, J.-J. Structural Determination of Zn and Pb Binding Sites in Penicillium Chrysogenum Cell Walls by EXAFS Spectroscopy. *Environ. Sci. Technol.* **1998**, *32* (11), 1648−1655.
(58) Ricachenevsky, F. K.; Menguer, P. K.; Sperotto, R. A.; Fett, J. P. Got to Hide Your Zn Away: Molecular Control of Zn Accumulation and Biotechnological Applications. *Plant Sci.* **2015**, *236*, 1−17.
(59) Sinclair, S. A.; Krämer, U. The Zinc Homeostasis Network of Land Plants. *Biochim. Biophys. Acta, Mol. Cell Res.* **2012**, *1823* (9), 1553−1567.
(60) Wang, P.; Menzies, N. W.; Lombi, E.; McKenna, B. A.; Johannessen, B.; Glover, C. J.; Kappen, P.; Kopittke, P. M. Fate of ZnO Nanoparticles in Soils and Cowpea (Vigna Unguiculata). *Environ. Sci. Technol.* **2013**, *47* (23), 13822−13830.

DOI: 10.1021/acsanm.8b01619
ACS Appl. Nano Mater. 2018, 1, 6414−6426